Agricultural Water Management 311 (2025) 109386

Contents lists available at ScienceDirect

Agricultural Water Management

journal homepage: www.elsevier.com/locate/agwat

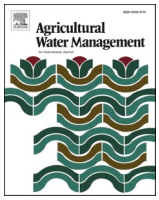

From weather data to water fluxes simulation in Mediterranean greenhouses through a combined climate and hydrological modelling approach

D. la Cecilia [a,*], A. Venezia [b], D. Massa [b], M. Camporese [a]

[a] Department of Civil, Environmental and Architectural Engineering, University of Padua, Padua, Italy
[b] CREA Research Centre for Vegetable and Ornamental Crops, Council for Agricultural Research and Economics, Via dei Cavalleggeri 51, Pontecagnano, SA 84098, Italy

ARTICLE INFO

Keywords:
Protected agriculture
Plastic greenhouse
Diplotaxis tenuifolia
Irrigation management

ABSTRACT

In the Mediterranean basin, agricultural land covered by greenhouses has been surging in the recent decades. The main goal of this study is to provide estimates of water demand and fluxes in Mediterranean greenhouses starting from outdoor weather data. This is achieved by developing a novel agricultural water modelling framework that combines a greenhouse climate model with a Richards equation-based hydrological model. We improve and evaluate an existing greenhouse climate model with greenhouse data from an experiment using rocket (*Diplotaxis tenuifolia*) as the candidate crop in South Italy for its market importance. The first major improvement regards the iterative estimation of the potential crop evapotranspiration using the FAO56 Penman Monteith method, adapted for greenhouse conditions, at the hourly scale, rather than a locally calibrated formula. The second one concerns the full coupling between the heat balance equations of the air and the soil compartments. The greenhouse climate model was able to simulate with satisfying accuracy the measured indoor air temperature (r^2=0.58 and KGE=0.76) and relative humidity (r^2=0.47 and KGE=0.67). Importantly, the crop potential evapotranspiration estimated from climate data either measured indoor or simulated with the greenhouse model were identical. Next, the hydrological model CATchment HYdrology (CATHY) was evaluated in the same experimental setting but different period (rocket in autumn and spring growing conditions), under sprinkler and subsurface drip irrigation. The CATHY model, fed with irrigation data and crop potential evapotranspiration estimated from measured indoor climate, reproduced well the measured soil water content dynamics at five depths (10, 20, 30, 40, 50 cm), despite some bias due to the lack of soil-specific sensor calibration. While the proposed modelling framework is currently coupled in a one-way manner, it has the potential to unlock valuable knowledge for the enhancement of our understanding of greenhouse farming implications on water management at plot and larger scales.

1. Introduction

Freshwater is a limiting factor in agriculture because evapotranspiration (ET) is often the largest component of the water balance (Ryken et al., 2022). Agriculture is already the sector that uses the largest share of water, achieving values of up to 69 % worldwide, on average (AQUASTAT, 2024). The depletion of freshwater resources will likely be exacerbated by the growing demand for food to meet the needs of an increasing human population and due to the projected increase of incoming solar longwave irradiance (Roderick et al., 2014). The latter is expected to drive an increase in crop transpiration (Mastrotheodoros et al., 2020) under well-watered conditions (Dong et al., 2022) and provided that excess air temperatures do not limit crop yield due to heat stress (Cammarano et al., 2022; Wang et al., 2017, 2020). Climate change is also driving more severe and frequent hazardous meteorological phenomena alternating from longer-lasting droughts to shorter and more intense rainfalls as well as increased seasonal variability in precipitation (Wade et al., 2022) that could strongly affect weather-related crop losses.

One technological solution allowing farmers to decouple crop production from meteorological conditions is offered by greenhouse cultivation. In its simplest form, greenhouses are built by covering soil-grown crops with plastic films supported by a metal frame, without an active climatic control, but with efficient irrigation systems (here referred to as

* Correspondence to: Department of Civil, Environmental and Architectural Engineering University of Padua, Padua 35131, Italy
E-mail address: daniele.lacecilia@unipd.it (D. la Cecilia).

https://doi.org/10.1016/j.agwat.2025.109386
Received 14 August 2024; Received in revised form 14 February 2025; Accepted 19 February 2025
Available online 2 March 2025
0378-3774/© 2025 The Author(s). Published by Elsevier B.V. This is an open access article under the CC BY license (http://creativecommons.org/licenses/by/4.0/).

plastic greenhouses) (Pérez Parra et al., 2004). Thanks to the possibility to control (at least partly) the indoor climate and to rely on less water, intensive vegetable production under plastic greenhouses thrives where sunlight is abundant, even in semi-arid environments (Baudoin et al., 2013; Goddek et al., 2023). For example, European-relevant districts of plastic greenhouses are located along the Mediterranean Sea coasts, such as the Almería region in Spain, the Anamur district in Turkey, the surroundings of Marina di Acate in Italy, and the Ierapetra district in Greece (la Cecilia et al., 2023a). Globally, other major clusters of greenhouse cultivation are found in China, Mexico and Morocco (Tong et al., 2024). Fernández et al. (2010) show that plastic greenhouses compared to open field agriculture can reduce ET from 1.5 mm day^{-1} down to 1 mm day^{-1} in winter and from 6.5 mm day^{-1} down to 4 mm day^{-1} in summer in Almería, Spain. The lower ET is mainly due to reduced solar radiation from outdoor to indoor (radiation transmission of about 60 %-70 %), further reduced with the use of whitening paint (radiation transmission of about 25 %-50 %) (Baille et al., 2001; Fernández et al., 2010). Moreover, in greenhouses the air relative humidity is high during the day and the wind speed is negligible, ranging between 0.1 and 0.3 m s^{-1} (Fernández et al., 2010). There are several equations for estimating evapotranspiration in greenhouses (Incrocci et al., 2020 and references therein). Those studies often corroborate that the FAO56 (Allen et al., 1998) methodology, recommended for open field conditions, is applicable to plastic greenhouses (Medrano et al., 2005) provided that indoor climate variables are used, and the coefficient of the aerodynamic resistance is equal to 295 s m^{-1} (Fernández et al., 2010). The lower ET achievable in plastic greenhouses implies lower irrigation water volumes, further reduced by adopting efficient irrigation systems, such as sprinkler or drip irrigation, controlled by expert knowledge and decision support systems (Berrueta et al., 2023; Gallardo et al., 2014).

In recent years, there has been a surge in mathematical models to improve greenhouse management and irrigation systems. On one hand, greenhouse climate models aim at estimating greenhouse crop transpiration, based on the simulation of indoor climate given outdoor weather and greenhouse management practices (references in Katzin et al., 2022). Measuring indoor climatic variables may be costly for low-income businesses and is typically not carried out by public agencies. By contrast, historical and forecast weather data for open field conditions are globally available. These data fed into a greenhouse climate model allow for estimating how much water the greenhouse crops require. This promises to increase food production in a water-efficient and optimal manner worldwide. The same interest is found in the context of open field agriculture, where scientists are resorting to optical and radar satellite data to quantify the volume of irrigation water used (Massari et al., 2021). However, these methods cannot be used for greenhouse cultivation for the plastic cover modifies the response of crops in the optical domain as well as the metal frame modifies the radar backscatter (la Cecilia et al., 2023a). On the other hand, hydrological models simulate soil water content (SWC) dynamics during the cropping season below plastic tunnels to study and improve the design of irrigation systems (Domínguez-Niño et al., 2020). These models resolve the water balance at the farm scale in space and time in a physically based manner, so that farmers and advisors can understand how to reduce water loss due to percolation and runoff by adapting irrigation management.

To better understand hydrological processes and to improve agricultural water resources management in greenhouse-dominated catchments, it is essential to develop a framework that combines greenhouse climate models with hydrological models. In this study, we selected and coupled in a one-way manner two existing greenhouse climate and hydrological models to develop and evaluate the potential of such a framework. We improve and use the greenhouse climate model proposed by Fitz-Rodríguez et al., (2010) to simulate indoor weather and ET given outdoor meteorological variables in a plastic greenhouse in the South of Italy in spring. Then, we evaluate the capability of the CATchment HYdrology (CATHY) model (Camporese et al., 2010) to simulate soil moisture dynamics in the same plastic greenhouse over two subsequent agricultural seasons and with two irrigation systems (i.e., sprinkler and subsurface drip irrigation). The main goal of this research is to demonstrate that the output of a greenhouse climate model can be used to feed hydrological models and, ultimately, to forecast irrigation water demand and optimize the irrigation strategy in greenhouse cultivation areas.

2. Methods

2.1. Study area

The study area is located in the *Piana del Sele* (Italy) (Fig. 1a), one of the largest production districts of vegetables in Italy and the main production area for some cut leafy vegetables, like rocket, in Europe. These fresh products are mostly cultivated in multi-tunnel plastic (polyethylene) greenhouses. The area is characterized by a Mediterranean climate. According to ERA5 data (Hersbach et al., 2023), yearly rainfalls sum up to nearly 1 000 mm concentrated in autumn and winter, with monthly averaged temperatures ranging between a minimum of 7 °C in January and a maximum of 31.5 °C in August.

With the aim of improving crop production and optimizing rocket fertigation, suitable data have been collected in an experimental greenhouse (Fig. 1b and c) located at the Research Centre for Vegetable and Ornamental Crops of the Council for Agricultural Research and Economics (CREA) (40° 38' 57" N 14° 53' 20" E). In particular, the experiment aimed at comparing two microirrigation systems for the delivery of the nutrient solution by sprinklers and drip irrigation in the spring of 2009 (Venezia et al., 2009), and by sprinklers and subsurface drip irrigation in the winter of 2010 and in the spring of 2011 (Venezia et al., 2011). The experimental greenhouse has a covered area of 480 m^2. It has roll-up side vents, with ground skirts to prevent cold air sweeping in, which are automatically controlled based on a user-defined air temperature threshold. The openings at the ridge roof were kept closed.

2.2. Greenhouse trial conditions

The greenhouse was split in two equal sectors using a plastic film from the ground up to the ridge pole and by ploughing a furrow of 50 cm depth. One sector was irrigated by sprinklers in 2009, 2010 and 2011, wetting an area of 3 m × 4 m with an irrigation rate of 25.0 mm h^{-1} (300 L h^{-1} per sprinkler) at an operational pressure of 3 atm. The other sector was irrigated by subsurface drip irrigation in 2010 and 2011, using auto-compensated dripper lines, positioned at 0.3 m on and between lines, at 30 cm depth, with an irrigation rate of about 13.3 mm h^{-1} (1.6 L h^{-1} per dripper) at an operational pressure of 1.2 atm.

The first of three experiments was carried out from 8 December 2008 to 24 April 2009 with four cuts made on 18 February, 16 March, 6 April and 24 April. However, the monitoring only covered the period from 1 April 2009 to 5 May 2009 for a total of 35 days. The second experiment was conducted from 14 October 2010 to the first cut on 3 December 2010 (51 days). The third experiment occurred from 29 April 2011 to the first cut on 31 May 2011 (33 days). Rocket (*Diplotaxis tenuifolia*) was sown with a plant density of 1 200 seeds m^{-2} in a silty soil ploughed and tilled as in commercial practices, obtaining raised beds 1.45 m wide, each spaced by 0.55 m (Fig. 1c).

Sprinkler irrigation was used as the only irrigation method in the first seven to ten days following sowing also in the experiments with subsurface drip irrigation, to allow for uniform and vigorous seed germination, plantlet emergence and rooting. An irrigation alert was triggered by a tensiometer (2725ARL Jet Fill) positioned in each sector at 10 cm depth with an intervention threshold of 0.3 atm. Irrigation volume was controlled manually. Only the cumulative irrigation volume was

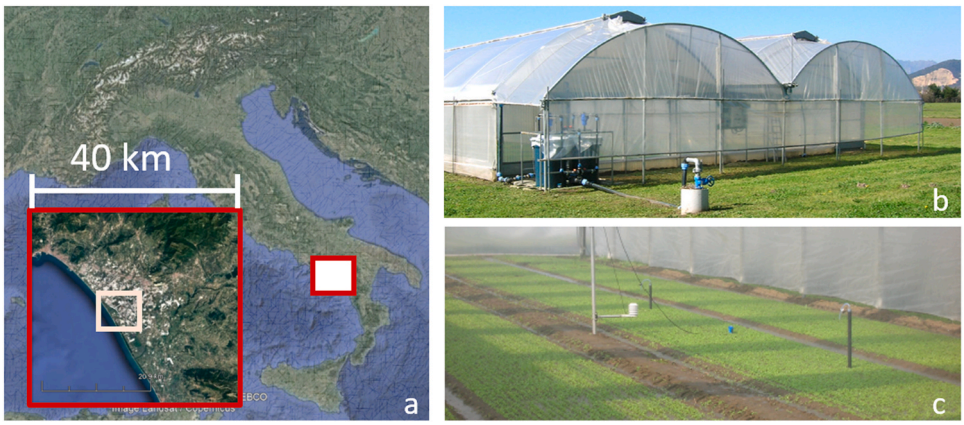

Fig. 1. a) Geographic location of the study area. b) Outside view of the experimental greenhouse. c) Inside view of the experimental greenhouse with the crop in its early stages, the indoor climate station (white pole), the tensiometers reading pore water pressure at 10 cm to trigger irrigation alerts and at 30 cm (black poles) and the Frequency Domain Reflectometry probes reading soil water content (SWC) at 10 cm, 20 cm, 30 cm, 40 cm and 50 cm to monitor irrigation (blue cap). The plastic film on the top right served to split the greenhouse in two equal sectors. Photos from the authors (Venezia et al., 2009, 2011).

recorded in the first experiment, while the irrigation time and volume were recorded in the last two experiments. In the second experiment, irrigation was given in excess to evaluate the soil leaching potential. In the last experiment, irrigation matched the reference evapotranspiration (ET_0) estimated as explained in subsection 2.4.

2.3. Outdoor hydro-meteorological data

The outdoor weather station mounted next to the experimental greenhouse recorded the air temperature (°C) and relative humidity (%) every 15 minutes. The hourly outdoor solar radiation (W m^{-2}) and wind speed (m s^{-1}) were retrieved from a nearby outdoor weather station (located at 40° 35' 5.6602" N 14° 58' 53.26" E – "stazione di Battipaglia") maintained by the Agriculture Office of the Campania region. The compiled dataset was used to calculate the outdoor hourly ET_O following the approach suggested by FAO for hourly input data (Allen et al., 1998) and implemented as in la Cecilia and Camporese (2022). Negative ET_O values, which might occur at nights or early mornings, were forced to 0 mm h^{-1}. The outdoor weather station had missing data, especially during wet weather. Missing data were filled with the corresponding hourly measurement of 24 hours earlier.

2.4. Indoor hydro-meteorological data

Frequency Domain Reflectometry (FDR) probes (EasyAG II® 50 cm TriSCAN by Campbell Scientific) were used to measure SWC (expressed in % v/v), using the factory calibration, at 10, 20, 30, 40 and 50 cm depth at 15-minute time resolution. Air temperature and relative humidity were monitored at crop canopy level with the same frequency of FDR measurements. Indoor solar radiation (W m^{-2}) was assumed to be a fixed percentage (70 %) of the measured outdoor solar radiation given the plastic cover characteristics. The reference evapotranspiration (mm h^{-1}) indoor was calculated following the approach suggested by FAO for hourly input data (Allen et al., 1998), and implemented as in la Cecilia and Camporese (2022), using indoor climate variables. Specifically for Mediterranean greenhouses, hourly input data are necessary for an accurate estimation of the reference evapotranspiration (Bonachela et al., 2024) and the coefficient of the aerodynamic resistance was set to 295 s m^{-1} (Fernández et al., 2010). Upon using a constant aerodynamic resistance, the wind speed does not appear in the Penman-Monteith equation for greenhouse. Moreover, Bonachela et al., (2023) suggest using an albedo of 0.16 rather than 0.23 to better estimate the daily net shortwave with crops like cucumber, melon and pepper. However, we kept the value of 0.23 because our crop was rocket, which is similar to grass. As for outdoor data, negative values were forced to 0 mm h^{-1}.

2.5. Development of the greenhouse climate model

The first experiment was used to test our improved version of the greenhouse climate model previously proposed by Fitz-Rodríguez et al. (2010), given the simultaneous availability of indoor and outdoor climate data. We chose this model for its comprehensiveness, validity, simplicity and transparency to simulate the "low-tech tunnel" type of greenhouses. The model parameters were sourced directly from Fitz--Rodriguez et al. (2010). The two improvements regard an iterative scheme to estimate ET based on the greenhouse climate and the two-way coupling between the air and soil modules. First, Eq. (1) was used to convert the relative humidity (RH) measured indoor (subscript $_{in}$ in place of $_k$) or outdoor (subscript $_{out}$ in place of $_k$) to the absolute humidity indoor (W_{in}) or outdoor (W_{out}), respectively:

$$W_k = \frac{RH_k}{100} \times \frac{0.611 \times e^{\frac{17.502 \times T_k}{T_k + 240.97}}}{\frac{T_k + 273.15}{18.02}} \times \frac{1000}{R_{gas} \times \rho_{air}} \quad (1)$$

Where R_{gas} is the universal gas constant (equal to 8.314 J mol^{-1} K^{-1}), ρ_{air} is the air density (kg m^{-3}) to convert the air absolute humidity from g-H_2O kg-dry-air^{-1} to g-H_2O m-air^{-3}. Eq. (1) was inverted to convert the calculated W_{in} to the measured RH_{in}, for validation. The model solves three ordinary differential equations, which are Eq. (2), Eq. (3) and Eq. (4), starting from the outdoor solar irradiance (Q_{GRout}), outdoor temperature (T_{out}) and W_{out}. The system returns the indoor air temperature (T_{in}), the indoor absolute humidity (W_{in}) and the ground surface temperature (T_f). The input hourly data were linearly interpolated to the time interval (dt) of 60 seconds and the equations were solved using the fourth-order Runge–Kutta method.

Indoor temperature T_{in} was calculated with Eq. (2):

$$\frac{dT_{in}}{dt} = \frac{1}{C_p \rho H}\left[Q_{GRin} + Q_{Heater} - L \bullet E - (T_{in} - T_{out}) \bullet (q_V C_p \rho + w \quad k)\right] - \frac{1}{C_s} \frac{1}{Z_0} h_S (T_{in} - T_f)\Big|_{t-1} \quad (2)$$

where, Q_{GRin} is the global radiation absorbed inside the greenhouse calculated as $Q_{GRout} \bullet \tau_c$, with τ_c being the solar radiation transmittance of the cover material (assumed equal to 0.7), C_p is the specific heat of moist air (1010 J kg^{-1} K^{-1}), ρ is the specific mass of air (1.2 kg-dry-air m^{-3}), H is the average greenhouse height (m), L is the latent heat of vaporization of water (2.5 $\times 10^6$ J kg^{-1}), q_V is the ventilation rate (m^3 m^{-2} s^{-1}), w is the ratio of glazing surface to floor surface (-), k is the heat transmission coefficient of glazing (J m^{-2} °C^{-1} h^{-1}), C_s is the heat capacity of the soil (2000 kJ m^{-3} °C^{-1}), Z_0 is the soil depth of the top layer

(0.05 m) and h_s is the heat transfer coefficient at soil surface (25.2 kJ m^{-2} °C^{-1} h^{-1}). The energy provided by heating or removed by cooling devices can be simulated with the variable Q_{Heater}; here, it was set to 0 W m^{-2} considering the lack of heating/cooling devices. The variable E may comprise water used for evaporative cooling, water lost for condensation and water generated by ET. In the experiments, neither evaporative cooling nor condensation was used and thus they were set to 0 g-H_2O m^{-2} s^{-1}. ET was not measured, and it was here calculated using the Penman-Monteith equation with indoor variables and aerodynamic parameters (subsection 2.4) in an iterative manner. Thus, ET corresponded to the maximum ET_0 possible based on the greenhouse climate, which in turn is affected by ET_0. The term $(T_{in} - T_{out}) \bullet (q_V C_p \rho)$ represents heat exchanges through ventilation and air drafts, while $(T_{in} - T_{out}) \bullet (w\ k)$ describes the conductive heat transfer between indoor and outdoor through the cover. Here, the model was improved to account for the two-way conductive heat exchange between indoor air and soil, acknowledging the soil contribution as heat storage, with the term $\frac{1}{C_s\ Z_0} h_S (T_{in} - T_f)\Big|_{t-1}$ calculated from the previous time step, just 60 s apart, for simplicity.

Indoor absolute humidity W_{in} was calculated with Eq. (3):

$$\frac{dW_{in}}{dt} = \frac{1}{\rho H}[E - (W_{in} - W_{out}) \bullet (q_V \rho)], \tag{3}$$

where all parameters and variables were already described for EQ1 and EQ2. RH_{in} was capped to 100 % in the model, thus programmatically removing any excess water generated by condensation, although it would affect the water and energy balance in the greenhouse.

Finally, Eq. (4) was used to calculate T_f and is written as:

$$\frac{dT_f}{dt} = \frac{1}{C_s\ Z_0}\left(\rho_g \alpha \frac{Q_{GRin}}{1000} + \varepsilon_a \varepsilon_f \sigma\left[(T_{in} + 273.15)^4 - (T_f + 273.15)^4\right] + h_S (T_{in} - T_f)\,|_{t-1} + \frac{k_S (T_{bl} - T_f) \bullet 2}{Z_0 + Z_1}\right), \tag{4}$$

ρ_g being the reflectance of the solar radiation on the ground (assumed to be 0.5), α the soil surface absorptivity (taken as 0.7), 1000 a unit conversion factor, ε_a the emissivity of air layer (equal to 0.75), ε_f the soil surface emissivity (equal to 0.95), σ the Stefan-Boltzmann constant (equal to 5.67 $\times 10^{-8}$ W m^{-2} K^{-4}), k_S the thermal conductivity of the soil (taken as 5.5 kJ m^{-1} °C^{-1} h^{-1}), T_{bl} the temperature at the boundary layer (considered at the interface between the soil depth of layer 0 and layer 1, i.e. 0.15 m), and Z_1 the soil depth of layer 1 (considered 10 cm). Given that soil temperature was not measured in the experiment, T_{bl} was assumed to be equal to 15 °C and it was not possible to validate T_f.

A large suite of climatic controls can be added to the model (Fitz-Rodríguez et al., 2010). Here, we accounted for the automatic opening/closing of the roll-up side vents based on a user-defined indoor air temperature threshold, which was set to 20 °C. The opening/closing is simulated via the increase/decrease of the ventilation rate (q_V).

Compared to the original greenhouse climate model by Fitz-Rodriguez et al. (2010), our improved version resulted in a more realistic simulation of the relevant variables (Figure S1). One difference was observed for the simulated air temperature, that was higher during the night, in the new version of the model, likely thanks to the included feedback from the soil heat term (Figure S1a). The other substantial difference was observed in terms of ET rates and cumulated depth, which were about four times higher in the new model, and more realistic, than in the original model formulation.

2.6. CATchment HYdrology (CATHY) model

In the latter two experiments, indoor weather and irrigation data were available. Therefore, these experiments were used to test the capability of the model CATHY to replicate the measured SWC at five depths. CATHY is a physics-based integrated surface-subsurface hydrological model (ISSHM), which simulates coupled water fluxes in the surface and subsurface, accounting for interactions with vegetation through the quantification of root water uptake. The subsurface module solves the 3D Richardson-Richards equation for variably saturated porous media with a finite element method (Camporese et al., 2010). The CATHY model uses the Feddes approach (Feddes et al., 1976; Camporese et al., 2015) to calculate the water stress function ∝ as a function of the pressure head ψ:

$$\propto(\psi) = \begin{cases} 0 \text{ when } \psi < \psi_{wp} \\ \dfrac{\psi - \psi_{wp}}{\psi_d - \psi_{wp}} \text{ when } \psi_{wp} < \psi < \psi_d \\ 1 \text{ when } \psi_d < \psi < \psi_{an} \\ 1 - \dfrac{\psi - \psi_{an}}{\psi_s - \psi_{an}} \text{ when } \psi_{an} < \psi < \psi_s \\ 0 \text{ when } \psi > \psi_s \end{cases} \tag{5}$$

where ψ_{wp} is the pressure head at the wilting point, ψ_d is the pressure head that starts causing stress to the vegetation, ψ_{an} is the anaerobiosis limit beyond which the plant starts to suffer excess soil water (i.e., oxygen deficiency) and ψ_s is the pressure head at saturation. By assuming that ET_0 is dominated by transpiration, CATHY calculates the actual ET based on the vegetation response as $ET_O \times \propto(\psi)$.

2.6.1. Model set-up

The texture of the soil under the greenhouse was analysed according to the USDA protocol in 2005. It was determined that the soil was a homogeneous loam from 0 cm to 90 cm (sand: 43.1 %, silt: 40.1 %, clay: 16.9 %, bulk density: 1.115 g cm^{-3}, field capacity: 0.226 cm^3 cm^{-3}, wilting point: 0.127 cm^3 cm^{-3}). The soil-crop system was modelled considering a 1.3 m^2 flat soil domain, with a horizontal discretization of 0.1 m to adequately represent the spacing between subsurface irrigation drippers. We modelled a total soil thickness of 5 m, assuming free drainage conditions as the bottom boundary condition given the lack of information on the depth of the water table. The soil thickness was discretized into thirty-six numerical layers parallel to the ground surface, with their thickness gradually increasing with depth. Soil depth intervals were equal to 2.5 cm from the surface to 60 cm depth, 10 cm from 60 cm to 1 m, and 50 cm down to the bottom. We assumed the presence of two soil horizons. The first between 0 cm and 20 cm where roots are mostly present and the second down to 5 m. Each soil layer is characterized by six hydraulic parameters (i.e., the specific storage coefficient, S_s, the saturated hydraulic conductivity, K_s, the porosity, φ, equal to the moisture content at saturation θ_s in CATHY, the residual moisture content, θ_r, and the two parameters of the Van Genuchten (1980) model, α and n, to calculate the volumetric SWC and unsaturated hydraulic conductivity as a function of the moisture content θ). The hydraulic soil parameters were estimated as described in subsection 2.6.2. Consistently with the fact that the soil was left bare prior to sowing, the crop coefficient, K_c, was assumed to be 0 in the first week after sowing, linearly increasing from 0 to 1 in the second week, and 1 afterwards, in all experimental conditions. The choice of K_c equal to 0 in the first week after sowing was made to retain a similarity with the equations by Fitz-Rodríguez et al., (2010), who prescribe ET= 0 mm when no vegetation is present. Even though values of 0.2 or more are recommended to account for bare soil evaporation (Allen et al., 1998), in our case, the difference in the results is not significant.

One full simulation typically lasts about 3 minutes on a personal laptop (intel CORE i7 8th Gen). We used indoor ET_0 calculated from measured indoor variables and the reported irrigation as boundary conditions at the surface, except for the case of subsurface drip irrigation, for which internal source terms (numerically equivalent to

Neumann boundary conditions in CATHY) were considered to provide irrigation at the locations of the subsurface drippers.

2.6.2. Model calibration

The soil hydraulic parameters of the two soil horizons were automatically calibrated with the Shuffled Complex Evolution algorithm (SCE-UA) (Duan et al., 1994), by searching for the best match between SWC simulated by CATHY at the five depths (10, 20, 30, 40 and 50 cm) and the corresponding measured values. In addition, we included in the calibration the unknown initial water table depth and assumed a hydrostatic pressure head profile. We assumed the parameters to be homogeneous and isotropic for each soil horizon. We kept constant the specific storage coefficient, at a value of 10^{-3} m^{-1}. The hydraulic parameters were first estimated using the ROSETTA3 pedotransfer function software (Zhang and Schaap, 2017) using the full list of needed soil variables (i.e., those measured in this study and reported in subsection 2.6.1). We obtained $K_s = 1.66 \times 10^{-5}$ m s^{-1}, $\varphi = 0.46$, $\theta_r = 0.06$, $\alpha = 2.32$ m^{-1} and $n = 1.37$. The period of interest, used to compute the

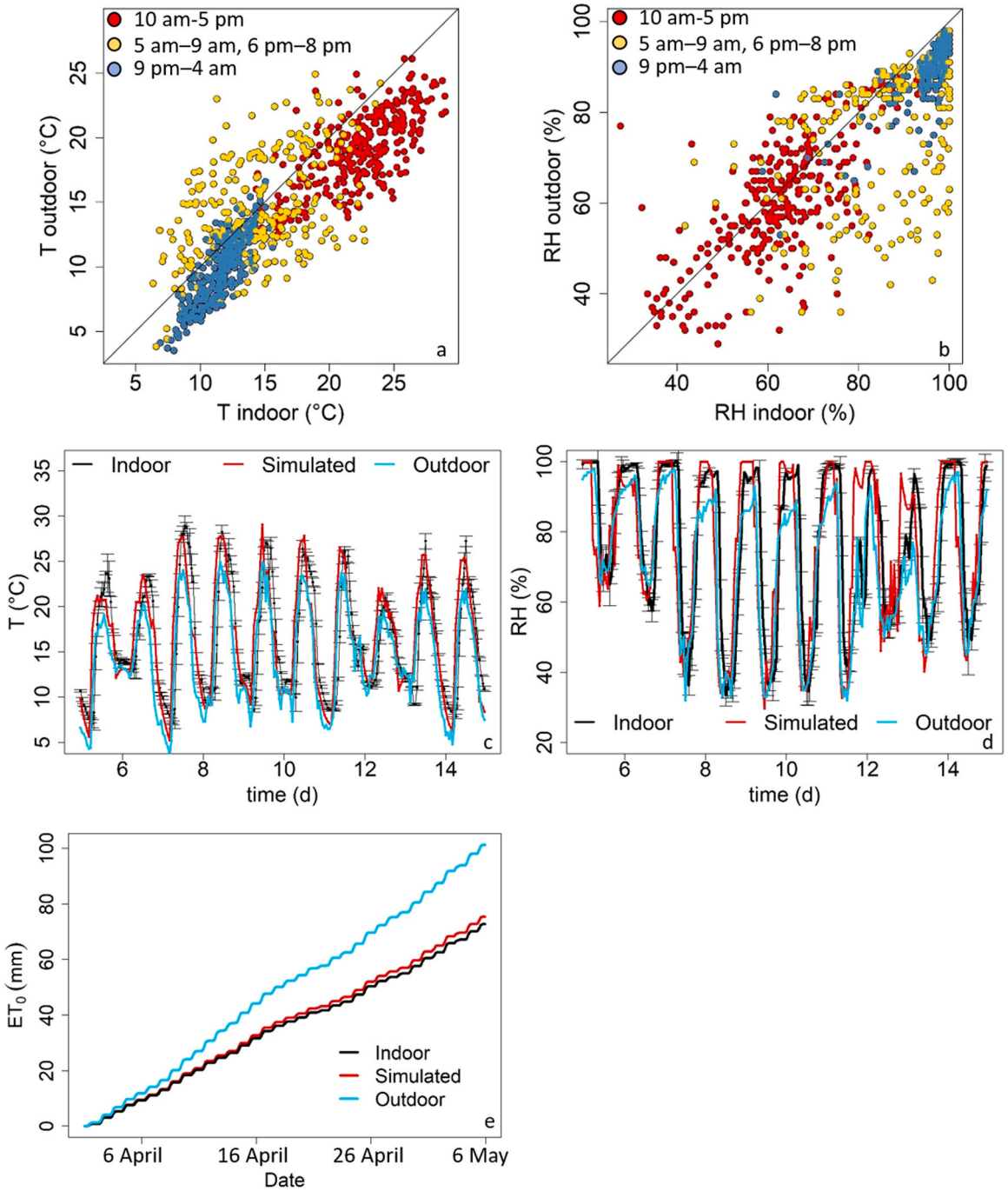

Fig. 2. Measured and simulated climate data. Panels a and b show the comparison between measured indoor and outdoor temperature (T) and relative humidity (RH), respectively. Data points are grouped by the time of the day and are depicted with circles filled in red (daytime from 10 am to 5 pm), yellow (sunrise from 5 am to 9 am and sunset from 6 pm to 8 pm) and nighttime (from 9 pm to 4 am). Panels c and d report the time series of measured indoor and outdoor temperature and relative humidity, as well as the simulated ones, zoomed in to the period between day 5 and day 15. Error bars relative to the measured data represent the standard deviation of 15 minutes resolution data when averaged to hourly values. Panel e displays the cumulative of the calculated reference evapotranspiration (ET_0) indoor, outdoor and indoor using simulated climate data.

goodness of fit, considered the first 24 days of the second experiment carried out in autumn under sprinkler irrigation condition, with simulation outputs being saved every four hours. The objective function to minimize was calculated as one minus the average Kling-Gupta Efficiency index (KGE) (Gupta et al., 2009), calculated between the measured and simulated SWC time series (interpolated at the same time points) for each of the five depths. The KGE index ranges between -∞ and 1, where a value of 1 indicates perfect agreement between the model predictions and the observed data. The KGE measures the accuracy of the model predictions against the observed data in terms of timing, bias and variability.

3. Results

3.1. Measured and simulated climate data

The first greenhouse experiment collected climate data indoor and outdoor in the period from 1 April 2009 to 6 May 2009. The indoor temperature was generally higher than the outdoor temperature (Fig. 2a), except for the time between 5 am and 9 am (yellow filled circles in Fig. 2a), when temperature was lower than the outside. The minimum indoor temperature at 50 cm height ranged between 6 °C and 13 °C and it was recorded at 7 am. The maximum temperature ranged between 15 °C and 28 °C and it was recorded at around 12 pm. Indoor relative humidity reached saturation levels at night as temperature dropped, and it decreased to values ranging between 40 % and 80 % in the day as temperature increased. Relative humidity was generally higher indoor than outdoor as more humid air was kept within the greenhouse (Fig. 2b).

The climate model was generally able to replicate the measured indoor temperature, with a coefficient of determination $r^2 = 0.58$ and KGE= 0.76, and to differentiate well from the outdoor temperature (red line in Fig. 2c). The model captured the daily dynamics of measured indoor relative humidity (Fig. 2d). However, the model simulated relative humidity less accurately than temperature, with a coefficient of determination $r^2 = 0.47$ and KGE= 0.67. The cumulative of the calculated ET_0 in indoor conditions was lower than the cumulative of the calculated ET_0 in outdoor conditions by about 40 % (Fig. 2e). The equation to calculate ET_0 differed only in the value of the aerodynamic resistance, which was 295 s m^{-1} instead of 208 s m^{-1} divided by the wind velocity at 2 m height, according to Fernández et al. (2010). Therefore, despite the higher indoor temperature, the remaining environmental factors must have predominated for the reduction of ET. These factors were lower irradiance, higher relative humidity and negligible wind speed. The contribution of each of these factors on the reduction of ET should be investigated contingent to the local climatic conditions and specific climate management operations. The calculated indoor ET_0 using measured or simulated climate data were in very good agreement with each other in terms of dynamics and magnitude (black and red lines, respectively, in Fig. 2e) and for hydrological modelling purposes can be used interchangeably. This result supports the use of the greenhouse climate model to estimate the potential evapotranspiration when measured indoor data lack.

3.2. Cumulative of reference evapotranspiration and irrigation

The second and third greenhouse experiments collected indoor climate and irrigation data in autumn, from 4 October 2010 to 3 December 2010, and in spring, from 29 April 2011 to 31 May 2011. Both seasons were tested under the two irrigation scenarios, sprinkler and

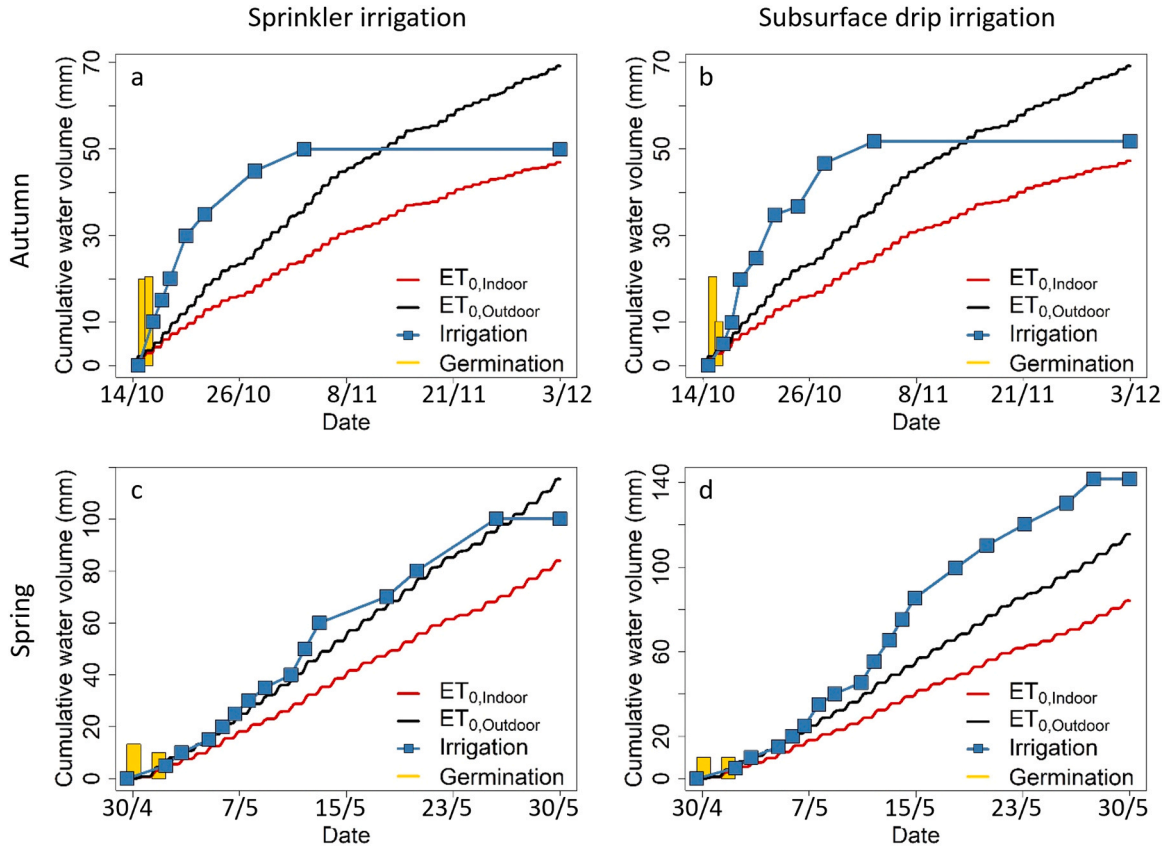

Fig. 3. Comparison between the cumulative of the calculated reference evapotranspiration (ET_0) indoor (red line) and outdoor (black line) with the cumulative of the irrigation volumes (blue line with squares) measured. The yellow bars indicate the volume of water provided for seed germination. Panel a refers to sprinkler irrigation in autumn and panel b to subsurface drip irrigation in autumn. Panel c refers to sprinkler irrigation in spring and panel d to subsurface drip irrigation in spring.

subsurface drip irrigation. In autumn, the total irrigation volume was 90 mm in nine events in the scenario with sprinkler irrigation (blue marked line in Fig. 3a) and 82 mm in ten events with subsurface drip irrigation (blue marked line in Fig. 3b). The first two irrigations with sprinklers used to ensure uniform and vigorous seed germination summed to about 40 mm in the sprinkler irrigation scenario and 30 mm in the subsurface drip irrigation scenario (yellow bars in Fig. 3a and b). In spring, the total irrigation volume was 123 mm in 15 events in the scenario with sprinkler irrigation (blue marked line in Fig. 3c) and 161 mm in 19 events with subsurface drip irrigation (blue marked line in Fig. 3d). The first two irrigations with sprinklers used to ensure uniform and vigorous seed germination summed to about 23 mm in the sprinkler irrigation scenario and 20 mm in the subsurface drip irrigation scenario (yellow bars in Fig. 3c and d).

Indoor ET calculated using measured indoor climate variables was always lower than outdoor ET calculated using weather data retrieved from the closest weather station located about 8 km away, as a comparison. Based on the ratio between ET indoor and outdoor, we can estimate water savings of about 60 % under greenhouse compared to open field conditions. The irrigation volume was always higher than indoor ET (comparison of red lines against blue marked lines in Fig. 3). This suggested that irrigation water was in excess, as it was designed in the autumn experiment. In spring, the irrigation volume intentionally followed the outdoor ET, limited to the sprinkler irrigation condition. In the subsurface drip irrigation condition, the irrigation volume was again in excess due to the tensiometer measuring low pressure head values at 10 cm and alerting the manager to irrigate.

3.3. Measured and simulated soil hydrological data

The second and third greenhouse experiments collected also SWC dynamics at five depths from 10 cm to 50 cm in autumn and spring. In the following, the results will be limited to the first 24 days of each experiment because that is the period when irrigation was provided. As it can be seen from the water content data at 50 cm, the irrigations for seed germination quickly reached the deeper soil layers in autumn (purple line in Fig. 4a and b). Afterwards, the signal of irrigation events continued to remain clearly visible at all depths given the excess irrigation strategy as well as because irrigation was provided in maximum one hour rather than, inevitably, over the whole evapotranspiration period. As expected, when subsurface drip irrigation started (day 8 in autumn, shown with gray vertical lines on the reversed y-axis in Fig. 4b), changes in SWC were larger from 20 cm depth down to deeper soil layers (orange, light blue, blue, and purple lines), but were not seen at 10 cm depth (green line). The comparison between measured SWC in the autumn period in the sprinkler irrigation and subsurface drip irrigation

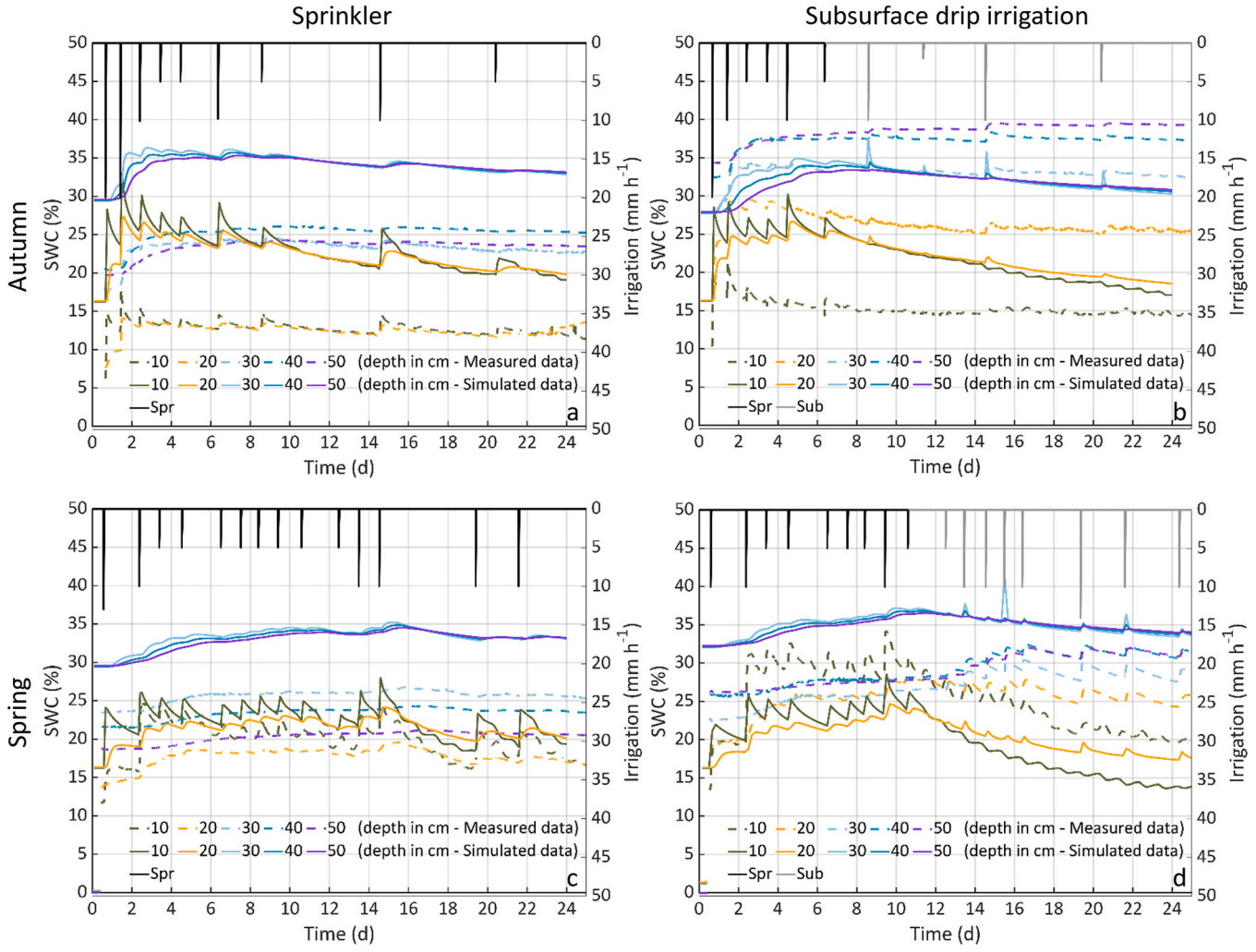

Fig. 4. Soil Water Content (SWC in %) measured and simulated for the sprinkler irrigation scenario (panels on the left) and subsurface drip irrigation scenario (panels on the right) in the last two cropping seasons (autumn in the panels on the top two rows and spring in the bottom two rows). Coloured lines represent the SWC at different depths reported in the legend in cm. Dashed lines depict measured data and continuous lines depict simulated values. Vertical lines on the reversed y-axis show the irrigation volume (mm h^{-1}) with sprinklers (Spr, in black) and subsurface drip irrigation (Sub, in gray).

scenarios indicated largely different initial conditions in the soil profiles of the two plots, despite being in the same greenhouse.

The measured SWC in the sprinkler irrigation scenario in autumn (Figure S1a) were adequately captured by the hydrologic simulation carried out with the soil hydraulic parameters computed with ROSETTA3 (Figure S1b, KGE = −0.15). However, the simulated SWC at the five depths showed, in general, a faster drainage and trends overlaid on each other, whereas the data clearly indicated differences between the SWC above 20 cm depth and the SWC below. In the best realization of the automatic calibration, the KGE index improved to 0.42 (Figure S1c), although the simulated SWC was still decreasing faster than the measured one. By analysing the KGE values for each soil depth and realization of the calibration process, we found that improving the KGE indices for the 10–20 cm soil depths was detrimental to the KGE indices of the 30–40–50 cm depths, and vice versa (Figure S2a). Eventually, we carried out a manual fine-tuning of the soil hydraulic parameters (Table 1). After the fine-tuning, CATHY replicated the SWC dynamics at all depths, but a substantial shift in the magnitude of the measured versus simulated SWC remained (KGE decreased to −0.09 in Fig. 4c and Figure S1d). We impute this shift, which likely impaired the calibration process, to the lack of in-situ calibration of the SWC sensors. Using the fine-tuned soil hydraulic parameters relative to the sprinkler irrigation scenario to simulate the subsurface drip irrigation scenario yielded somehow satisfactory results because the SWC dynamics were captured as well as the subsurface irrigation events (KGE=-0.58, in Fig. 4d). Considering the different initial conditions between the two irrigation scenarios in the same season and greenhouse it was clear that the subsurface drip irrigation scenario would require a separate calibration to improve the simulations of the measured SWC. It is possible that the construction of the subsurface drip irrigation system impacted the soil hydraulic properties but also that the SWC probes required a site-specific calibration.

In the spring period, the less abundant and more frequent irrigation events resulted in clearly visible SWC dynamics at 10 cm and 20 cm depths (green and orange lines), but not at deeper soil layers (light blue, blue, and purple lines) in the sprinkler irrigation scenario (Fig. 4c) and in the subsurface drip irrigation one (Fig. 4d). In the subsurface drip irrigation scenario, from day 12, the SWC was maintained or increased only below 20 cm depth as the irrigation method changed (gray vertical lines on the reversed y-axis in Fig. 4d). In the subsurface drip irrigation scenario, there were SWC diel fluctuations, much evident in the top soil (green line) and less evident below, in autumn (Fig. 4b) and in spring (Fig. 4d). In the top soil, the SWC maxima were reached in the early afternoon, while below they were reached in the evening. While it has been shown that temperature amplifies the diurnal changes of SWC (Nasta et al., 2024; Varble and Chávez, 2011), the SWC diel fluctuations could also be the result of ET dynamics, with crops taking up soil water only during the day, causing lower SWC during the day and higher SWC at night in deeper soil layers (la Cecilia and Camporese, 2022). The initial conditions in terms of SWC were again different between the two scenarios. This is again unexpected given that soil was left untouched, from 3 December 2010 to 29 April 2011, between the trials in the two seasons. Once again, a likely reason for the different initial conditions is the lack of site-specific SWC probes calibration.

The spring period was simulated using the fine-tuned soil hydraulic parameters estimated in the sprinkler irrigation scenario in autumn. The model CATHY was able to replicate well the dynamics of the measured SWC at all depths in the sprinkler irrigation scenario (Fig. 4c, KGE=0.34), although the bias in the SWC magnitude was detrimental to the accuracy. The subsurface drip irrigation scenario was again affected by the shift in the magnitude of the measured versus simulated SWC (KGE = −0.43 in Fig. 4d). The capability of CATHY to describe subsurface drip irrigation further allows for spatially visualizing the SWC along the three directions in the soil (Fig. 5), thus enhancing the understanding of irrigation water flow paths and redistribution.

Table 1
Fine-tuned soil hydraulic parameters values used in the simulations. Specific storage coefficient kept to 1.00×10^{-3} m^{-1}.

Depth (cm)	Hydraulic conductivity (m s^{-1})	Porosity (-)	Residual moisture content (-)	van Genuchten - n (-)	van Genuchten - α (m^{-1})
0–20	5.64×10^{-6}	0.41	0.06	1.53	1.75
20–500	1.76×10^{-5}	0.46	0.02	1.22	1.54

4. Discussions

4.1. Greenhouse climate model

Most of the greenhouse climate models published in the scientific literature consider the greenhouse a perfectly stirred tank (Katzin et al., 2022), similarly to the model developed in this study, improved after Fitz-Rodríguez et al. (2010). Under this assumption, transient effects caused by the spatial variability of any variables are disregarded. As a consequence, our model was not able to simulate the indoor temperature at the location of the sensor during the thermal inversion that occurred inside the greenhouse between 5 am and 9 am, when the indoor temperature was lower than outside (yellow filled circles in Fig. 2a). In this context, Lee et al., (2019) show that the location of an air temperature sensor to monitor the indoor climate matters. Similarly, climatic changes due to air ventilation may take a while before indoor conditions reach again the state of a perfectly stirred tank. The current 0-D formulation of the presented greenhouse climate model cannot adequately describe the complex relationship between air ventilation rate, vent openings, and heat losses. For example, Ould Khaoua et al. (2006) use a calibrated computational fluid dynamic model to reveal that different openings configuration and outdoor wind speed can result in differences between 2 °C and 6 °C inside the greenhouse. The lack of a perfect match between the simulated and measured indoor climate variables could also be explained by the fact that plastic greenhouses are not air-tight when closed. For instance, Baille et al. (2006) determined a total convective heat transfer by leakage up to 43 W m^{-2} and determined that the leakage was proportional to the outdoor wind speed. It follows that a better description of the ventilation rate and leakage is needed in the future development of the greenhouse climate model for improving its accuracy. More complex models exist, which still assume well-mixed conditions (Katzin et al., 2022). For example, the model KASPRO (De Zwart, 1996), a commercial software, includes more variables not only to include more processes but also to more realistically represent how heat is exchanged between the outside and inside of the greenhouse, and vice versa. However, here the focus is on open-source models, for the sake of data reproducibility.

Increased complexity can also be found in another type of greenhouse models, such as those based on computational fluid dynamics. These models allow for fully describing the building geometry and the indoor environment in the three spatial dimensions and over time (Norton et al., 2007). However, they are computationally demanding and need expert users to be set up and run. While this latter class of models is needed for understanding air flows in greenhouses (Ould Khaoua et al., 2006), we deemed them impractical for the purpose of the modelling framework developed in this study, which is intentionally parsimonious.

Relative humidity also depends on temperature. Therefore, the greatest discrepancies between measured and simulated indoor relative humidity was reached in the early day during thermal inversion. Moreover, only ET_0 and ventilation were included as the processes regulating the dynamics of water vapour, while others were not. We recall that ET_0 at each time step was calculated according to Penman-Monteith (Allen et al., 1998), and adjusted as in Fernández et al. (2010) for greenhouses. As a major improvement of our climate model,

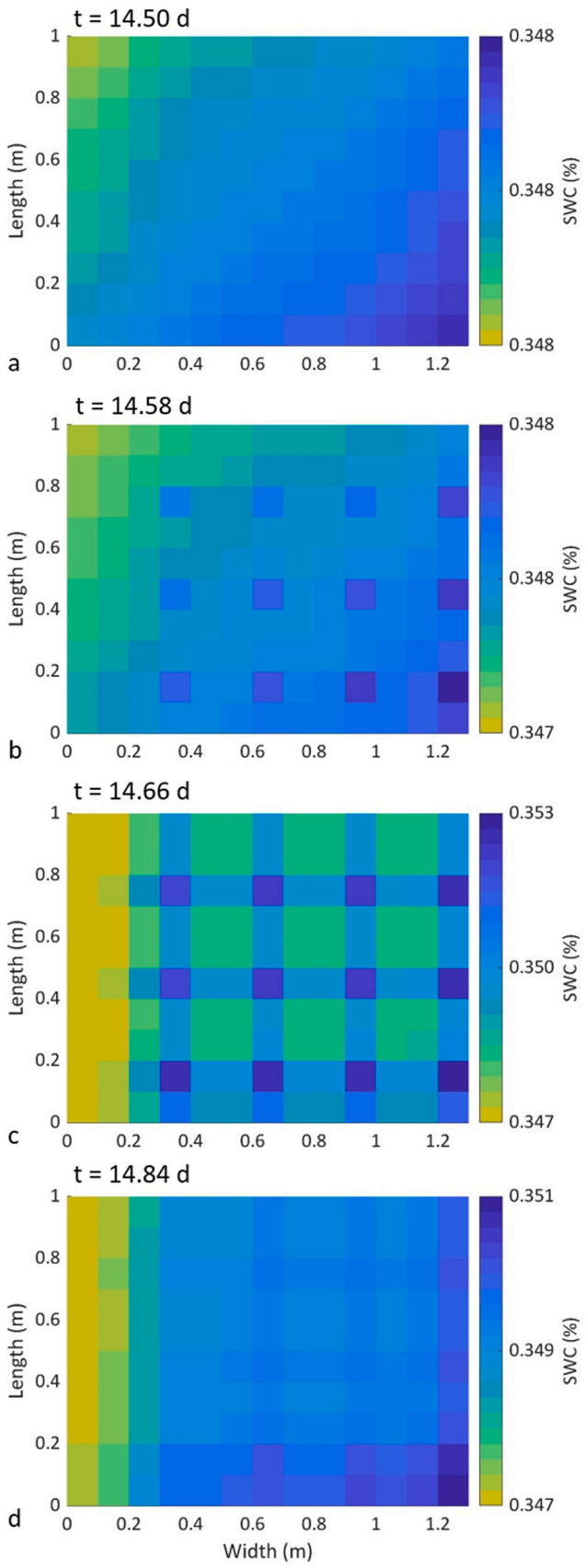

Fig. 5. Spatial distribution of soil water content (SWC in %) at 40 cm depth, from just before subsurface drip irrigation (a) and then at four hours intervals (b to d). The first three columns on the left of the grid represent the spacing between raised beds, so they were left bare, without irrigation and ET.

ET_0 calculation is based on an iterative procedure that fed back the value of ET_0 on the greenhouse climate, for they influence each other. This procedure allows for calculating the maximum ET_0 possible at those climate conditions, although an actual time series of ET_0 values (not available in this study) could be fed in the model to possibly achieve a higher accuracy in the validation. Regarding the adjustment to the coefficient of the aerodynamic resistance proposed by Fernández et al. (2010), it followed that the wind speed, or air circulation rate, in the greenhouse had a constant value of 0.7 m s^{-1}. This may overestimate ET_0 since typical air circulation rates achieve 0.3 m s^{-1}. However, when the greenhouse roll-up side vents are open, it is likely that the wind speed may be higher than the air circulation rates and moist exchanges will depend on the complex relationship between wind speed and the openings (Ould Khaoua et al., 2006). ET_0 is a relevant variable in the context of greenhouse management and it can be estimated with a plethora of models (Katsoulas and Stanghellini, 2019). The more simplistic formulations to calculate ET_0 are linear functions of the irradiance and they are generally locally calibrated (e.g., Fernández et al., 2010). Formulations more complex than a Penman-Monteith approach (Allen et al., 1998) would include the roles of CO_2 concentration and of light spectrum on crop phenology (such as in the KASPRO model by De Zwart, 1996). Indeed, CO_2 can be injected inside the greenhouse to boost the growth of suitable crops. However, CO_2 injection is not a common practice in low-tech plastic greenhouses, such as the one considered in this study, and, therefore, this process was not included. The additional advantage of calculating ET_0 with a process-based crop model would be the opportunity to simulate the crop yield, which may spark interest in using the model by a wider audience of practitioners and agronomists. There are two more processes that are relevant not only to possibly improve the model accuracy but also to have an impact on the management of the greenhouse from the climatic and crop protection points of view. These processes are irrigation and condensation. Sprinkler irrigation, rather than subsurface drip irrigation, can be considered as a source of water and latent heat, which was neglected in this study given the difficulty to quantify its role. Yet, evaporative cooling, which is nothing but a short sprinkler irrigation, is sometimes a strategy to lower the indoor temperature in arid climates (Goddek et al., 2023). As far as subsurface drip irrigation is concerned, Phogat et al. (2016) propose an adaptation of the Penman Monteith approach to account for the lower soil evaporation in vineyards. However, for mature rocket the crop coefficient is wholly explained by transpiration. Thus, we hypothesized that the irrigation system did not require a modification of the Penman Monteith approach in our case. Given the importance of temperature and humidity on greenhouse control, these processes shall be systematically addressed in the future by collecting more data in the greenhouse.

4.2. Soil hydrology

Several topics of interest emerge from the analyses of measured and simulated SWC dynamics. These topics concern the irrigation volumes used for seed germination, the need for sensor-specific calibration for interdisciplinary hydrological applications, and the applications of hydrological models as well as proximal sensing technology to optimally manage irrigation.

The acquired irrigation data revealed that the ratio between inputs for seeds germination and those to meet the crop demand were on average 0.40 in the sprinkler irrigation scenario and 0.15 in the subsurface drip irrigation scenario. These high ratios imply that irrigation water for seed germination was a significant component of the water inputs. A similar tendency of excess water use with respect to crop demand up to 2–5 times for crop establishment, followed by adequate water use during crop growth, was found by Fernández et al. (2007). Still, some excess water may be applied to prevent an increase in soil salinity depending on the irrigation water quality, assure a uniform application and to avoid that some plants are water-limited (Incrocci

et al., 2020). Therefore, there is a need to transfer this knowledge to other spheres pertaining to water resources management, which typically neglect these practices (Abbott et al., 2019; Valmassoi and Keller, 2022), to improve water inputs estimation in hydrological modelling at large spatial scales. Although it is still common practice to irrigate in excess as discussed above, or to follow the crop manager experience as it was tested in this study, there is room, and need, to save irrigation water with an optimal irrigation scheduling based on the estimation of crop water demand or the actual SWC (Incrocci et al., 2020), or the use of decision support systems (De Pascale et al., 2018; Navarro et al., 2023). On one side, the estimation of crop water demand is carried out using formulas to calculate ET_0, and the implications were presented in subsection 3.2 and discussed in subsection 4.1. There exist also relatively new approaches that enable direct, real-time acquisition of the plant's water use by measuring the sap flow, and thus to adjust irrigation accordingly (Navarro et al., 2023; Vurro et al., 2023). On the other side, SWC sensors enable to schedule irrigation volumes and timings when the measured SWC reaches user-defined critical values for crop health. The capacity to evaluate the actual water availability in the root zone has led to a widespread use of this technology (Varble and Chávez, 2011) and could eventually lead to improved water use efficiency based on artificial intelligence-driven autonomous control of irrigation (Hemming et al., 2019; Nikolaou et al., 2019).

In farming, it may suffice to acquire the SWC using factory-calibrated sensors to trigger irrigation based on user-defined SWC thresholds. Nonetheless, there exist applications for which accurate values of soil water content are of paramount importance for understanding and modelling land-atmosphere water and energy exchanges, and their feedback on related earth processes (Seneviratne et al., 2010). For this, several studies highlighted the necessity to carry out individual sensor-, soil- and location- specific calibrations (Varble and Chávez, 2011; Zawilski et al., 2023) and recommended to account for soil temperature in the calibration (Nasta et al., 2024; Varble and Chávez, 2011), particularly for clayey soils. Based on those studies, we imputed the shift in magnitude of the measured versus simulated SWC in our study to the lack of calibration of the SWC sensors, given that the dynamics were well simulated. The bias remained also after testing several metrics for error minimization, such as the root mean square error and the Nash-Sutcliffe Efficiency index (Nash and Sutcliffe, 1970). The experience gained in the experimental greenhouse showed that scheduling irrigation based on the tensiometer sensors positioned in the top 10 cm led to excess water use, given that the SWC sensors located below the root zone registered increased SWC, indicating the occurrence of leaching. Therefore, it is recommended to install one sensor in the root zone, ideally at the centre of the wet bulb (Bonachela et al., 2018), and one below the root zone to monitor any leaching. This recommendation is of particular importance should subsurface drip irrigation be used (Raij-Hoffman et al., 2024), given that water is already provided in the soil profile.

The application of SWC sensors for large-scale monitoring, beyond the plot level, may be unfeasible. While they can provide important real-time data, they cannot be directly extrapolated into the future. To overcome these limitations, hydrological modelling allows water managers to design optimal irrigation practices based on the irrigation technology, crop management, soil conditions and climatic scenarios (Domínguez-Niño et al., 2020; Skaggs et al., 2004). The capability of models to describe subsurface drip irrigation (e.g., CATHY as in this study or HYDRUS from Skaggs et al., 2004 to Raij-Hoffman et al., 2024) is of crucial importance for they visualize the spatial variability and changes of SWC in the soil (Fig. 5), thus enhancing the understanding of irrigation water flow paths and redistribution. These capabilities are not only essential to optimize water use but also to prevent/track the leaching of nutrients and plant protection products present in the soil or in the irrigation water to the water table, which may eventually reach surface water also in dry periods (la Cecilia et al., 2023b). However, also numerical simulations have their caveats at small spatial scales. One relevant consideration regards the necessity to estimate the soil hydraulic parameters to produce accurate outputs. In our study, the estimated soil hydraulic parameters did not yield accurate SWC values (still, we stress the fact that the SWC sensors were not calibrated, which had an impact on parameters' estimation), although the time dynamics was well captured. Therefore, when applying the model to other locations, one would necessitate to acquire SWC data to estimate the local soil hydraulic parameters. Skaggs et al., (2004) suggest that hydraulic parameters can be estimated using the ROSETTA pedotransfer function software (e.g., Zhang and Schaap, 2017). Our simulations agree with Domínguez-Niño et al., (2020), who conclude that ROSETTA is suitable for predicting SWC trends; still, site-specific estimation of hydraulic parameters is necessary to improve the simulations accuracy. We also found the need for test-specific calibration in our study, where, in particular, the construction of the subsurface irrigation system likely impacted the soil. Another challenge for SWC data validation particularly relevant in subsurface drip irrigation was the possibility that the emitters became clogged or did not discharge water uniformly, which cannot be readily seen in the field (Lamm and Camp, 2007; Rodríguez-Sinobas et al., 2021). Here, geoelectrical measurements, used as proxies of SWC, can help quantifying the temporal and spatial dynamics of SWC in the root zone (Chou et al. 2024; Mary et al., 2021; Raij-Hoffman et al., 2024; Vanella et al. 2023).

4.3. Advantages and limitations of the proposed modelling framework

The modelling framework can find quick and widespread applicability in areas within the Mediterranean basin highly impacted by greenhouses. This is because the greenhouse model used parameters sourced from the literature (Fitz-Rodriguez et al., 2010) and only the ventilation rate was manually calibrated. Also, the hydrological model could already be run quite accurately with soil hydraulic parameters estimated with the ROSETTA software (Zhang and Schaap, 2017) from known soil properties, which is a typically available information to farmers. The framework has great potential for water resources management. It is based on the same logic of current hydrological applications, where it is common to apply boundary conditions (i.e., evapotranspiration) and use empirical functions (i.e., Feddes et al., 1976) to control the feedback with the soil hydrology. Despite the advantages of the modelling framework, it is currently based on a one-way coupling. The main consequence is that there is no feedback between the soil temperature, which the greenhouse model simulates, and the soil hydrology. Soil temperature influences soil evaporation, with the latter being inherently controlled by the available soil moisture. This mechanism is currently not implemented in the framework and will be the subject of future model development. Put into a broader context, the greenhouse model will not be affected by the lack of soil moisture, simulated by the hydrological model, in the estimation of the evapotranspiration.

5. Conclusions

In this study, we proposed a comprehensive modelling framework that simulates water fluxes in plastic greenhouses starting from outdoor weather conditions. The framework consists of a one-way coupling of a greenhouse climate model and a Richards equation-based hydrological model. The greenhouse model was developed to simulate, within a feedback loop, the air temperature, relative humidity, soil temperature, and evapotranspiration inside the greenhouse given outdoor weather conditions. It is a 0-D parsimonious model that was evaluated here against climate data measured under a plastic greenhouse and achieved adequate accuracy for the simulated variables. The evapotranspiration rates calculated using measured indoor climate data were identical to those calculated by the model. Therefore, we conclude the model is suitable to estimate the evapotranspiration rates to be used in hydrological models. However, due to the 0-D formulation of the climate model, it would fail where strong spatial gradients exist, for instance

during the transient conditions following the activation of controlling devices. Then, the physics-based hydrological model can be interchangeably fed with measured or simulated indoor boundary conditions to simulate soil water content in the same greenhouse setting with sprinkler and subsurface drip irrigation. The performance of the hydrological model to simulate measured soil water content at different depths was also adequate. Overall, the results show that the proposed modelling framework can be used by scientists and practitioners to analyse and optimize water management in protected agriculture. Future studies will be needed using data from different geographical regions, climate, and seasons of the year to understand the robustness and transferability of both models. Meanwhile, multiple improvements, starting from the two-way feedback between the models and the role of sprinkler irrigation as a source of heat and moist in greenhouses, will be implemented and tested. The continue improvement of the framework grounds on the acquisition of new data, and would greatly benefit from a collective effort and FAIR datasets.

Declaration of Competing Interest

The authors declare that they have no known competing financial interests or personal relationships that could have appeared to influence the work reported in this paper.

Acknowledgements

This research is part of the MSCA-PF project REWATERING and received funding from the European Union's Horizon Europe research and innovation programme under the Marie Skłodowska-Curie grant agreement No. 101062255. The experiments in the greenhouse were funded by the Campania Region (DRD 354 del 28.07.08 and DRD 162 del 30.03.10). We thank the five anonymous reviewers whose insightful comments allowed us to greatly improve the clarity and quality of the manuscript.

Appendix A. Supporting information

Supplementary data associated with this article can be found in the online version at doi:10.1016/j.agwat.2025.109386.

Data availability

Data and models can be found in the Research Data Unipd repository at 10.25430/researchdata.cab.unipd.it.00001493. The CATHY model is freely available at https://bitbucket.org/cathy1_0/cathy/.

References

Abbott, B.W., Bishop, K., Zarnetske, J.P., et al., 2019. Human domination of the global water cycle absent from depictions and perceptions. Nat. Geosci. 12, 533–540. https://doi.org/10.1038/s41561-019-0374-y.

Allen, R.G., Pereira, L.S., Raes, D., Smith, M., 1998. Crop evapotranspiration (guidelines for computing crop water requirements). FAO Irrig. Drain. Pap. No. 56. 1–333.

AQUASTAT, 2024. AQUASTAT - FAO's Global Information System on Water and Agriculture. ⟨https://www.fao.org/aquastat/en/overview/methodology/water-use⟩ (accessed 01 May 2024).

Baille, A., Kittas, C., Katsoulas, N., 2001. Influence of whitening on greenhouse microclimate and crop energy partitioning. Agric. For. Meteorol. 107, 293–306.

Baille, A., López, J.C., Bonachela, S., González-Real, M.M., Montero, J.I., 2006. Night energy balance in a heated low-cost plastic greenhouse. Agric. For. Meteorol. 137, 107–118. https://doi.org/10.1016/j.agrformet.2006.03.008.

Baudoin, W., Nono-Womdim, R., Lutaladio, N., Hodder, A., Castilla, N., Leonardi, C., De Pascale, S., Qaryouti, M., Duffy, R., 2013. Good Agricultural Practices for greenhouse vegetable crops. Principles for Mediterranean climate areas, FAO PLANT PRODUCTION AND PROTECTION PAPER, 217.

Berrueta, C., Grasso, R., García, C., Thompson, R.B., Gallardo, M., 2023. Use of the VegSyst model to simulate seasonal dry matter production, N and K uptake and evapotranspiration in greenhouse soil-grown tomato in Uruguay. Agric. Water Manag., 108395 https://doi.org/10.1016/j.agwat.2023.108395.

Bonachela, S., Fernández, M.D., Cabrera, F.J., Granados, M.R., 2018. Soil spatio-temporal distribution of water, salts and nutrients in greenhouse, drip-irrigated tomato crops using lysimetry and dielectric methods. Agric. Water Manag. 203, 151–161. https://doi.org/10.1016/j.agwat.2018.03.009.

Bonachela, S., Fernández, M.D., Hernández, J., López, J.C., 2023. Adaptation of standardised (FAO and ASCE) procedures of estimating net longwave and shortwave radiation to Mediterranean greenhouse crops. Biosyst. Eng. 231, 104–116.

Bonachela, S., Fernández, M.D., Hernández, J., Karaca, C., 2024. Computing air temperature and humidity for reference crop evapotranspiration calculation in passive Mediterranean greenhouses. Agric. Water Manag. 302. https://doi.org/10.1016/j.agwat.2024.108991.

Cammarano, D., Jamshidi, S., Hoogenboom, G., Ruane, A.C., Niyogi, D., Ronga, D., 2022. Processing tomato production is expected to decrease by 2050 due to the projected increase in temperature. Nat. Food 3, 437–444. https://doi.org/10.1038/s43016-022-00521-y.

Camporese, M., Paniconi, C., Putti, M., Orlandini, S., 2010. Surface subsurface flow modeling with path-based runoff routing, boundary condition-based coupling, and assimilation of multisource observation data. W02512 Water Resour. Res. 46. https://doi.org/10.1029/2008WR007536.

Camporese, M., Daly, E., Paniconi, C., 2015. Catchment-scale Richards equation-based modeling of evapotranspiration via boundary condition switching and root water uptake schemes. Water Resour. Res. 51, 5756–5771. https://doi.org/10.1002/2015WR017139.

la Cecilia, D., Camporese, M., 2022. Resolving streamflow diel fluctuations in a small agricultural catchment with an integrated surface-subsurface hydrological model. Hydrol. Process. 36, e14768. https://doi.org/10.1002/hyp.14768.

la Cecilia, D., Dax, A., Ehmann, H., Koster, M., Singer, H., Stamm, C., 2023b. Continuous high-frequency pesticide monitoring in a small tile-drained agricultural stream to reveal diel concentration fluctuations in dry periods. Front. Water 4, 1062198. https://doi.org/10.3389/frwa.2022.1062198.

la Cecilia, D., Tom, M., Stamm, C., Odermatt, D., 2023a. Pixel-based mapping of open field and protected agriculture using constrained Sentinel-2 data. ISPRS Open J. Photogramm. Remote Sens. 8, 100033. https://doi.org/10.1016/j.ophoto.2023.100033.

Chou, C., Peruzzo, L., Falco, N., Hao, Z., Mary, B., Wang, J., Wu, Y., 2024. Improving evapotranspiration computation with electrical resistivity tomography in a maize field. Vadose Zone J. 23, e20290. https://doi.org/10.1002/vzj2.20290.

De Pascale, S., Rouphael, Y., Gallardo, M., Thompson, R.B., 2018. Water and fertilization management of vegetables: state of art and future challenges. Eur. J. Hortic. Sci. 83, 306–318. https://doi.org/10.17660/eJHS.2018/83.5.4.

De Zwart, H.F., 1996. Analyzing Energy-Saving Options in Greenhouse Cultivation Using a Simulation Model. Landbouwuniversiteit, Wageningen.

Domínguez-Niño, J.M., Arbat, G., Raij-Hoffman, I., Kisekka, I., Girona, J., Casadesús, J., 2020. Parameterization of Soil Hydraulic Parameters for HYDRUS-3D Simulation of Soil Water Dynamics in a Drip-Irrigated Orchard. Water (7), 1858. https://doi.org/10.3390/w12071858.

Dong, J., Akbar, R., Short Gianotti, D.J., Feldman, A.F., Crow, W.T., Entekhabi, D., 2022. Can surface soil moisture information identify evapotranspiration regime transitions? Geophys. Res. Lett. 49, e2021GL097697. https://doi.org/10.1029/2021GL097697.

Duan, Q., Sorooshian, S., Gupta, V.K., 1994. Optimal use of the SCE-UA global optimization method for calibrating watershed models. J. Hydrol. 158, 265–284.

Feddes, R.A., Kowalik, P., Kolinska-Malinka, K., Zaradny, H., 1976. Simulation of field water uptake by plants using a soil water dependent root extraction function. J. Hydrol. 31, 13–26.

Fernández, M.D., González, A.M., Carreño, J., Pérez, C., Bonachela, S., 2007. Analysis of on-farm irrigation performance in Mediterranean greenhouses. Agric. Water Manag. 89, 251–260. https://doi.org/10.1016/j.agwat.2007.02.001.

Fernández, M.D., Bonachela, S., Orgaz, F., Thompson, R., López, J.C., Granados, M.R., Gallardo, M., Fereres, E., 2010. Measurement and estimation of plastic greenhouse reference evapotranspiration in a Mediterranean climate. Irrig. Sci. 28, 497–509. https://doi.org/10.1007/s00271-010-0210-z.

Fitz-Rodríguez, E., Kubota, C., Giacomelli, G.A., Tignor, M.E., Wilson, S.B., McMahon, M., 2010. Dynamic modeling and simulation of greenhouse environments under several scenarios: A web-based application. Comput. Electron. Agric. 70, 105–116. https://doi.org/10.1016/j.compag.2009.09.010.

Gallardo, M., Thompson, R.B., Giménez, C., Padilla, F.M., Stöckle, C.O., 2014. Prototype decision support system based on the VegSyst simulation model to calculate crop N and water requirements for tomato under plastic cover. Irrig. Sci. 32, 237–253. https://doi.org/10.1007/s00271-014-0427-3.

Goddek, S., Körner, O., Keesman, K.J., Tester, M.A., Lefers, R., Fleskens, L., Joyce, A., van Os, E., Gross, A., Leemans, R., 2023. How greenhouse horticulture in arid regions can contribute to climate-resilient and sustainable food security. Glob. Food Secur., 100701 https://doi.org/10.1016/j.gfs.2023.100701.

Gupta, H.V., Kling, H., Yilmaz, K.K., Martinez, G.F., 2009. Decomposition of the mean squared error and NSE performance criteria: implications for improving hydrological modelling. J. Hydrol. 377, 80–91. https://doi.org/10.1016/j.jhydrol.2009.08.003.

Hemming, S., de Zwart, F., Elings, A., Righini, I., Petropoulou, A., 2019. Remote control of greenhouse vegetable production with artificial intelligence—greenhouse climate, irrigation, and crop production. Sensors 19, 1807. https://doi.org/10.3390/s19081807.

Hersbach, H., Bell, B., Berrisford, P., Biavati, G., Horányi, A., Muñoz Sabater, J., Nicolas, J., Peubey, C., Radu, R., Rozum, I., Schepers, D., Simmons, A., Soci, C., Dee, D., Thépaut, J.-N., 2023: ERA5 hourly data on single levels from 1940 to present. Copernicus Climate Change Service (C3S) Climate Data Store (CDS), doi:10.24381/cds.adbb2d47 (Accessed 12 May 2024).

Incrocci, L., Thompson, R.B., Fernández, M.D., De Pascale, S., Pardossi, A., Stanghellini, C., Rouphael, Y., Gallardo, M., 2020. Irrigation management of

European greenhouse vegetable crops. Agric. Water Manag. 242, 106393. https://doi.org/10.1016/j.agwat.2020.106393.
Katsoulas, N., Stanghellini, C., 2019. Modelling crop transpiration in greenhouses: different models for different applications. Agronomy 9, 392. https://doi.org/10.3390/agronomy9070392.
Katzin, D., van Henten, E.J., van Mourik, S., 2022. Process-based greenhouse climate models: Genealogy, current status, and future directions. Agric. Syst. 198, 103388. https://doi.org/10.1016/j.agsy.2022.103388.
Lamm, F.R., Camp, C.R., 2007. Subsurface drip irrigation. "Micro Crop Prod. Des., Oper., Manag." 13, 473–551.
Lee, S., Lee, I., Yeo, U., Kim, R., Kim, J., 2019. Optimal sensor placement for monitoring and controlling greenhouse internal environments. Biosyst. Eng. 188, 190–206. https://doi.org/10.1016/j.biosystemseng.2019.10.005.
Mary, B., Peruzzo, L., Iván, V., Facca, E., Manoli, G., Putti, M., Camporese, M., Wu, Y., Cassiani, G., 2021. Combining models of root-zone hydrology and geoelectrical measurements: recent advances and future prospects. Front. Water 3, 767910. https://doi.org/10.3389/frwa.2021.767910.
Massari, C., Modanesi, S., Dari, J., Gruber, A., De Lannoy, G.J.M., Girotto, M., Quintana-Seguí, P., Le Page, M., Jarlan, L., Zribi, M., et al., 2021. A review of irrigation information retrievals from space and their utility for users. Remote Sens 13, 4112. https://doi.org/10.3390/rs13204112.
Mastrotheodoros, T., Pappas, C., Molnar, P., Burlando, P., Manoli, G., Parajka, J., Rigon, R., Szeles, B., Bottazzi, M., Hadjidoukas, P., Fatichi, S., 2020. More green and less blue water in the Alps during warmer summers. Nat. Clim. Change 10, 155–161. https://doi.org/10.1038/s41558-019-0676-5.
Medrano, E., Lorenzo, P., Sánchez-Guerrero, M.C., Ignacio Montero, J., 2005. Evaluation and modelling of greenhouse cucumber-crop transpiration under high and low radiation conditions. Sci. Hortic. 163–175. https://doi.org/10.1016/j.scienta.2005.01.024.
Nash, J.E., Sutcliffe, J.V., 1970. River flow forecasting through conceptual models part I: A discussion of principles. J. Hydrol. 10, 282–290.
Nasta, P., Coccia, F., Lazzaro, U., Bogena, H.R., Huisman, J.A., Sica, B., Mazzitelli, C., Vereecken, H., Romano, N., 2024. Temperature-Corrected Calibration of GS3 and TEROS-12 Soil Water Content Sensors. Sensors 24, 952. https://doi.org/10.3390/s24030952.
Navarro, A., Scotto di Covella, F., Cacini, S., Sodini, M., Traversari, S., Venezia, A., Massa, D., 2023. Testing sap-flow sensors to predict irrigation of soilless tomato fertigated with saline water. Acta Hortic. (1377). https://doi.org/10.17660/ActaHortic.2023.1377.78.
Nikolaou, G., Neocleous, D., Katsoulas, N., Kittas, C., 2019. Irrigation of Greenhouse Crops. Hortic 5, 7. https://doi.org/10.3390/horticulturae5010007.
Norton, T., Sun, D., Grant, J., Fallon, R., Dodd, V., 2007. Applications of computational fluid dynamics (CFD) in the modelling and design of ventilation systems in the agricultural industry: a review. Bioresour. Technol. 98, 2386–2414. https://doi.org/10.1016/j.biortech.2006.11.025.
Ould Khaoua, S.A., Bournet, P.E., Migeon, C., Boulard, T., Chassériaux, G., 2006. Analysis of greenhouse ventilation efficiency based on computational fluid dynamics. Biosyst. Eng. 95, 83–98. https://doi.org/10.1016/j.biosystemseng.
Pérez Parra, J., Baeza, E., Montero, J.I., Bailey, B.J., 2004. Natural ventilation of parral greenhouses. Biosyst. Eng. 87, 355–366. https://doi.org/10.1016/j.biosystemseng.2003.12.004.
Phogat, V., Šimůnek, J., Skewes, M.A., Cox, J.W., McCarthy, M.G., 2016. Improving the estimation of evaporation by the FAO-56 dual crop coefficient approach under subsurface drip irrigation. Agric. Water Manag. 178, 189–200. https://doi.org/10.1016/j.agwat.2016.09.022.
Raij-Hoffman, I., Vanella, D., Ramírez-Cuesta, J.M., Peddinti, S.R., Kisekka, I., 2024. Detecting soil water redistribution in subsurface drip irrigated processing tomatoes using electrical resistivity tomography, proximal sensing and hydrological modelling. Sci. Tot. Environ. 912, 169620. https://doi.org/10.1016/j.scitotenv.2023.169620.
Roderick, M.L., Sun, F., Lim, W.H., Farquhar, G.D., 2014. A general framework for understanding the response of the water cycle to global warming over land and ocean. Hydrol. Earth Syst. Sci. 18, 1575–1589. https://doi.org/10.5194/hess-18-1575-2014.
Rodríguez-Sinobas, L., Zubelzu, S., Martín-Sotoca, J.J., Tarquis, A.M., 2021. Multiscaling analysis of Soil Water Content during irrigation events. Comparison between surface and subsurface drip irrigation. Geoderma 382, 114777. https://doi.org/10.1016/j.geoderma.2020.114777.
Ryken, A.C., Gochis, D., Maxwell, R.M., 2022. Unravelling groundwater contributions to evapotranspiration and constraining water fluxes in a high-elevation catchment. Hydrol. Process. 36, e14449. https://doi.org/10.1002/hyp.14449.
Seneviratne, S.I., Corti, T., Davin, E.L., Hirschi, M., Jaeger, E.B., Lehner, I., Orlowsky, B., Teuling, A.J., 2010. Investigating soil moisture-climate interactions in a changing climate: a review. Earth Sci. Rev. 99, 125–161. https://doi.org/10.1016/j.earscirev.2010.02.004.
Skaggs, T.H., Trout, T.J., Šimůnek, J., Shouse, P.J., 2004. Comparison of HYDRUS-2D simulations of drip irrigation with experimental observations. J. Irrig. Drain. Eng. 130, 304–310. https://doi.org/10.1061/~ASCE!0733-9437–2004!130:4–304!.
Tong, X., Zhang, X., Fensholt, R., Rosendal, P., Jensen, D., Li, S., Larsen, M.N., Reiner, F., Tian, F., Brandt, M., 2024. Global area boom for greenhouse cultivation revealed by satellite mapping. Nat. Food 5, 513–523. https://doi.org/10.1038/s43016-024-00985-0.
Valmassoi, A., Keller, J.D., 2022. A review on irrigation parameterizations in Earth system models. Front. Water 4, 906664. https://doi.org/10.3389/frwa.2022.906664.
Van Genuchten, M.T., 1980. A closed form equation for predicting the hydraulic conductivity of unsaturated soils. Soil Sci. Soc. Am. J. 44, 892–898.
Vanella, D., Ramírez-Cuesta, J.M., Longo-Minnolo, G., Longo, D., D'Emilio, A., Consoli, S., 2023. Identifying soil-plant interactions in a mixed-age orange orchard using electrical resistivity imaging. Plant Soil 483, 181–197. https://doi.org/10.1007/s11104-022-05733-6 (Eds.).
Varble, J.L., Chávez, J.L., 2011. Performance evaluation and calibration of soil water content and potential sensors for agricultural soils in eastern Colorado. Agric. Water Manag. 101, 93–106. https://doi.org/10.1016/j.agwat.2011.09.007.
Venezia, A., Bacco, A., Caponigro, V., Chiancone, I., Di Cesare, C., Farina, M., Landi, A., Stipic, M., Piro, F., 2009. Relazione su coltivazione a basso impatto ambientale per la produzione di rucola da quarta gamma, Consiglio per la ricerca e la sperimentazione in agricoltura.
Venezia, A., Caponigro, V., Chiancone, I., Comella, S., Di Cesare, C., Farina, M., Landi, A., Stipic, M., 2011. Relazione sul secondo saggio di coltivazione a basso impatto ambientale per la produzione di rucola da quarta gamma, Consiglio per la ricerca e la sperimentazione in agricoltura.
Vurro, F., Manfredi, R., Bettelli, M., et al., 2023. In vivo sensing to monitor tomato plants in field conditions and optimize crop water management. Precis. Agric. 24, 2479–2499. https://doi.org/10.1007/s11119-023-10049-1.
Wade, C.M., Baker, J.S., Van Houtven, G., Cai, Y., Lord, B., Castellanos, E., Leiva, B., Fuentes, G., Alfaro, G., kondash, A.J., henry, C.L., Shaw, B., Redmon, J.H., 2022. Opportunities and spatial hotspots for irrigation expansion in Guatemala to support development goals in the food-energy-water nexus. Agric. Water Manag. 267, 107608. https://doi.org/10.1016/j.agwat.2022.107608.
Wang, E., Martre, P., Zhao, Z., et al., 2017. The uncertainty of crop yield projections is reduced by improved temperature response functions. Nat. Plants 3, 17102. https://doi.org/10.1038/nplants.2017.102.
Wang, X., Zhao, C., Müller, C., et al., 2020. Emergent constraint on crop yield response to warmer temperature from field experiments. Nat. Sustain 3, 908–916. https://doi.org/10.1038/s41893-020-0569-7.
Zawilski, B.M., Granouillac, F., Claverie, N., Lemaire, B., Brut, A., Tallec, T., 2023. Calculation of soil water content using dielectric-permittivity-based sensors - benefits of soil-specific calibration. Geosci. Instrum. Methods Data Syst. 12, 45–56. https://doi.org/10.5194/gi-12-45-2023.
Zhang, Y., Schaap, M.G., 2017. Weighted recalibration of the Rosetta pedotransfer model with improved estimates of hydraulic parameter distributions and summary statistics (Rosetta3). J. Hydrol. 547, 39–53. https://doi.org/10.1016/j.jhydrol.2017.01.004.